

# Distributed Reed-Solomon Coded Cooperative Space-Time Labeling Diversity Network

Chen CHEN<sup>1</sup>, Fengfan YANG<sup>1</sup>, Chunli ZHAO<sup>1</sup>, Hongjun XU<sup>2</sup>

<sup>1</sup> College of Electronics and Information Engg., Nanjing Univ. of Aeronautics and Astronautics, Nanjing, 210016 China

<sup>2</sup> School of Engineering, University of KwaZulu-Natal, King George V Avenue, Durban, 4041, South Africa

chenchen05182020@163.com, yffee@nuaa.edu.cn, chunlizhao\_cn@163.com, xuh@ukzn.ac.za

Submitted May 16, 2022 / Accepted September 8, 2022 / Online first October 7, 2022

**Abstract.** *This paper proposes a distributed Reed-Solomon coded cooperative labeling diversity (DRSCC-LD) scheme over the Rayleigh frequency-flat fast fading channel to further improve the BER performance. The non-binary Reed-Solomon (RS) code with more consecutive roots is applied at the relay to provide additional redundancy. As a novel diversity technique, labeling diversity (LD) with three different mappers is employed in the proposed DRSCC-LD scheme utilizing 16-QAM and 64-QAM, respectively, which may achieve diversity gain and greatly decrease the error floor (EF). Besides, a reduced-complexity detection algorithm based on a variable signal subset (RC-VSS) is proposed to lower the complexity of detection at both relay and destination. The proposed critical SNR-assisted (CSA) joint decoding algorithm then collaborates with the joint detection based on the RC-VSS algorithm to improve the overall BER performance. Theoretical analysis and Monte Carlo simulated results reveal that the proposed DRSCC-LD scheme clearly outperforms its corresponding non-cooperative RS coded scheme by a gain of more than 7 dB and the existing schemes by a margin of more than 3.5 dB under the identical conditions, respectively.*

## Keywords

Reed-Solomon (RS) code, distributed coded cooperation, labeling diversity (LD), detection algorithm, joint decoding algorithm

## 1. Introduction

Recently, multiple-input multiple-output (MIMO) as an efficient technique has been widely applied to increase the data rates, link reliability, and spectral efficiency of the wireless communication system [1]. In MIMO communication schemes, Bit-Interleaved Space-Time Coded Modulation with an Iteratively Decoding system (BI-STCM-ID) [2] is an attractive scheme that provides both space-time diversity gain and coding gain. Nevertheless, the average error

performance of the BI-STCM-ID scheme is significantly dependent on the labeling mapper [3], a function that assigns the bitstreams to the constellation point. Hence, the design of the labeling mappers has garnered substantial interest in the research community. In [4], Y. Huang et al. demonstrated an optimal label map that maximizes the Euclidean distance between two labels with the one-bit difference in the BI-STCM-ID scheme. Furthermore, Y. Huang et al. [5] also presented an improved 16-QAM labeling approach for BI-STCM-ID using the Alamouti space-time block coding (STBC). M. Krasicki et al. [6] proposed a better labeling technique known as Labeling Diversity (LD) for BI-STCM whose iterative decoding is employed at the receiver with two different label mappers. This novel scheme has resulted in promising bit-error-rate (BER) performance gains and a reduction in the error floor (EF) region when compared to the transmission systems without labeling diversity [7].

Meanwhile, the concept of coded cooperative diversity, which can be viewed as a virtual MIMO system for mobile devices, was first proposed by Van der Meulen [8] and has proven to be a more efficient means of combating the channel impairments in the transmission and can achieve a greater diversity gain than the existing amplify-and-forward (AF) and detect-and-forward (DF) cooperative diversity [9]. Typically, a coded cooperative system consists of three terminals: a source S, a relay R, and a common destination D. S and R jointly construct a better resultant code at D than point-to-point communication transmission, resulting in a superior BER performance. Therefore, several channel codes such as turbo codes [10], Reed-Muller codes [11], LDPC codes [12], [13] and polar codes [14], [15] have been distributed to the coded cooperative communication systems. Moreover, the high order of Quadrature Amplitude Modulation (QAM) can be applied in the practical coded-cooperation scheme to increase bandwidth efficiency. However, the BER performance degrades drastically as the modulation order increases. Consequently, the aforementioned LD technique may effectively generate a symbiotic relationship between modulation techniques and code construction, demonstrating the rationality and validity of the coded cooperation in conjunction with LD technology. In fact, LD has been implemented

in the relay networks. In [16], the authors explored distributed turbo codes and LDPC codes based on LD, which has yielded significant BER performance by the application of LD at the source node, therefore significantly lowering the risk of relay outage in the coded-cooperative scheme. Ejaz S et al. [17] also proposed LD for single-antenna cooperative communication schemes. Nevertheless, the aforementioned LD communication systems only focus on binary codes based on BPSK modulation. Research on coded cooperation based on non-binary codes has not been thoroughly investigated. Reed-Solomon (RS) code is a well-known non-binary maximum distance separable (MDS) code that corrects random burst errors. Compared with Turbo code and LDPC code close to the Shannon limit, RS code can achieve a good compromise between BER performance and decoding complexity under the condition of short-to-medium code length. Therefore, RS code has been an excellent candidate for application in various practical communication systems including coded-cooperative communications [18]. In [19], Guo et.al. have proposed an efficient construction approach for optimizing the RS code at the destination. However, the poor EF region and bandwidth efficiency occur in the actual scenarios, which are demonstrated in their work. These challenges provide the primary motivation for this paper. Meanwhile, Zhao et.al. [20] proposed the RS-coded cooperative transmission scheme that employs space-time block coded spatial modulation (STBC-SM) to enhance bandwidth efficiency. Nevertheless, the joint RS code acquired at the destination may have a bad free distance due to the random information selection at the relay, which influences the error-correction capability of the overall scheme. Additionally, the EF region has not been diminished yet. Based on the previous research, the authors further address the existing issues in RS-coded cooperation. Inspired by the application of MIMO to coded cooperation and the advantages of LD, the authors propose the distributed RS coded cooperative labeling diversity (DRSCC-LD) scheme which combines RS coding with LD and utilizes the construction approach introduced in [19]. Moreover, a novel joint decoding algorithm is proposed, which illustrates a superior BER performance than the existing algorithms in papers [19] and [20].

Therefore, the main contributions of this manuscript are concluded as follows:

- The distributed  $3 \times 3$  WLAN coded cooperative network employs the space-time LD technique for the first time in conjunction with non-binary RS codes, i.e., the proposed DRSCC-LD scheme. Moreover, the novel information selection approach provided in [19] is applied at the relay to optimize the construction of the resultant code at the destination.
- Theoretical error performance analysis for both the non-cooperative RS coded scheme and the DRSCC-LD scheme is derived and verified by the numerical simulations.
- A reduced-complexity detection algorithm based on a variable signal subset (*RC-VSS*) is developed to bal-

ance the BER performance and the detection complexity, and then, the joint detection at the destination based on the *RC-VSS* algorithm is explored.

- A novel critical SNR-assisted (*CSA*) joint decoding algorithm is proposed to utilize at the destination for further enhancing the BER performance.
- The proposed DRSCC-LD scheme is evaluated not only in ideal circumstances but also in practical (non-ideal) scenarios.

The remaining structure of this manuscript is organized as follows. Section 2 introduces the generalized distributed coded cooperation. Then, the DRSCC-LD scheme is proposed based on the generalized model in Sec. 3. Section 4 details the derivation of the theoretical average bit error probability (ABEP) of the DRSCC-LD scheme. Section 5 introduces the optimal maximum likelihood (ML) detection and further proposes the *RC-VSS* detection algorithm. Based on this algorithm, the joint detection approach is then developed. Subsequently, a novel *CSA* joint decoding is elaborated in Sec. 6. Section 7 presents the numerical simulations of the proposed DRSCC-LD scheme over the Rayleigh frequency-flat fast fading channel. Finally, Section 8 concludes this paper.

## 2. Generalized Distributed Space-Time Coded Cooperative Scheme

The generalized coded cooperative communication transmission model was first introduced by Van der Meulen [8], which is comprised of three terminals: the source  $S$ , the relay  $R$ , and the destination  $D$ . The distributed space-time coded cooperation scheme is illustrated in Fig. 1. Trivially, each terminal contains two antennas to receive and send the signals taking two-time slots in a half-duplex model with the premise that the antennas are sufficiently separated to minimize mutual interference.

During the 1<sup>st</sup> time slot, the message sequence  $\mathbf{u}_1$  is encoded by the 'Encoder 1' of channel code  $C_S$ . In this paper, the authors employ a non-binary RS code encoder that will be introduced in Sec. 3. Then, the encoded information data are sent to the 'Space-time diversity' module that modulates the binary message vector (symbols need to be converted to bitstreams) to the space-time codeword  $\mathbf{X}_S$  and subsequently transmits to the relay and destination simultaneously over the radio frequency (RF) channel. Note that LD is applied to this module in the proposed DRSCC-LD scheme, which will be elaborated in Sec. 3. Furthermore, the received signals are denoted as  $\mathbf{Y}_{S-R}$  and  $\mathbf{Y}_{S-D}$  at the relay and destination, respectively, and be modeled as:

$$\mathbf{Y}_{S-R} = \mathbf{H}_{S-R}\mathbf{X}_S + \mathbf{N}_{S-R}, \quad (1.a)$$

$$\mathbf{Y}_{S-D} = \mathbf{H}_{S-D}\mathbf{X}_S + \mathbf{N}_{S-D} \quad (1.b)$$

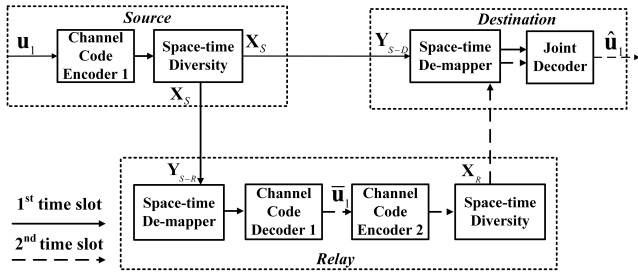


Fig. 1. Generalized distributed space-time coded cooperation model.

where  $\mathbf{X}_S$  is a  $N_T \times Q$  matrix,  $Q$  is the number of time intervals required to transmit one space-time codeword,  $N_T$  is the number of transmit antennas,  $\mathbf{H}_{S-R}$  and  $\mathbf{H}_{S-D}$  are the  $N_R \times N_T$  Rayleigh fading channel matrices between source to relay and destination, respectively,  $N_R$  is the number of receive antennas, and  $\mathbf{N}_{S-R}$  and  $\mathbf{N}_{S-D}$  are  $N_R \times Q$  Gaussian noise matrices. Note that each entry of  $\mathbf{H}_{S-R}$  and  $\mathbf{H}_{S-D}$  are independent and identically distributed (i.i.d) complex Gaussian random variables (RVs) that follow  $CN(0, 1)$  and the items of  $\mathbf{N}_{S-R}$  and  $\mathbf{N}_{S-D}$  are also i.i.d complex Gaussian RVs satisfying  $CN(0, \sigma^2)$ ,  $\sigma^2$  is the power spectral density (PSD) of noise. Then, the received signal  $\mathbf{Y}_{S-R}$  passes to the 'Space-time De-mapper' block and the 'Channel Code Decoder 1' block of  $C_S$  in sequence to recover the message symbol/bit sequence  $\bar{\mathbf{u}}_1$  where  $\bar{\mathbf{u}}_1$  may not equal to  $\mathbf{u}_1$  due to the different conditions of the S-R link (if the S-R link is ideal, then  $\bar{\mathbf{u}}_1 = \mathbf{u}_1$ ).

During the 2<sup>nd</sup> time slot, through the 'Channel Code Encoder 2' module of the channel code  $C_R$ , the relay re-encodes  $\bar{\mathbf{u}}_1$ . Then, the resultant information sequence is sent to the space-time diversity block to become the space-time codeword  $\mathbf{X}_R$ . Similarly,  $\mathbf{X}_R$  is propagated to the destination over RF channel where the received signal is denoted  $\mathbf{Y}_{R-D}$  and modeled as:

$$\mathbf{Y}_{R-D} = \mathbf{H}_{R-D}\mathbf{X}_R + \mathbf{N}_{R-D} \quad (2)$$

where  $\mathbf{H}_{R-D}$  and  $\mathbf{N}_{R-D}$  are also the fading channel and additive white Gaussian noise (AWGN) matrices defined identically as  $\mathbf{H}_{S-D}$  and  $\mathbf{N}_{S-D}$ , respectively. Ultimately,  $\mathbf{Y}_{S-D}$  and  $\mathbf{Y}_{R-D}$  are both demodulated during each time slot in the 'space-time de-mapper' block at the destination. The detected signals are transmitted to the joint decoder subsequently to recover the final estimated message sequence  $\hat{\mathbf{u}}_1$ . Presented above is a brief introduction to the distributed space-time coded-cooperation, and the specific modeling process of our proposed scheme will be explained in Sec. 3.

### 3. Proposed Distributed RS Coded Cooperative LD (DRSCC-LD) Scheme

In this section, the schematic of the proposed DRSCC-LD scheme is illustrated in Fig. 2, where RS encoding and LD technique are employed in the channel code and space-time diversity blocks, respectively, to reduce the complexity

of decoding and the EF region, and then further improve the BER performance. Different from the traditional LD scheme [16], this paper first proposes a  $3 \times 3$  MIMO system ( $N_T = N_R = 3$ ) with three distinct labeling mappers of 16-QAM and 64-QAM modulation schemes employed in neighboring space streams to improve error performance. In addition, the design of three distinct mappers for M-ary phase shift keying (M-PSK) [21] and M-ary amplitude phase shift keying (M-APSK) [22] modulation schemes are preliminarily investigated, which will be explored in the further study. Therefore, in this paper, the M-QAM modulation scheme is focused on. Furthermore, two different RS codes are distributed at the source and relay, respectively, where another highlight is the selection of information symbols at the relay. Moreover, DRSCC-LD also retrieves the information at the destination through two phases similar to the generalized model.

In the first phase, the binary information sequence  $\mathbf{u}_1$  is first converted to the  $M$ -ary symbols  $\mathbf{m}_1$  of length  $K_1$  at the source where  $M$  is the modulation order. In this paper,  $M = 16$  or  $64$  are considered due to the optimized labeling mappers in LD and the feature of the short-to-medium-length information transmission of RS code [18]. Subsequently,  $\mathbf{m}_1$  is encoded to the systematic RS codeword  $\mathbf{c}_1$  of length  $N$  by the  $RS_1(N, K_1, d_1)$  encoder where the free/minimum distance  $d_1 = N - K_1 + 1$ . Note that the modulation order  $M$  determines the code length  $N$  of the RS code in this paper, which is  $N = 15$  or  $63$ . Moreover, the generator polynomial of  $RS_1$  is provided as follows, comprising of  $N - K_1$  consecutive power of a primitive element  $\alpha \in GF(2^n)$ :

$$\mathbf{g}_1(x) = (x - \alpha)(x - \alpha^2) \cdots (x - \alpha^{N-K_1}) \quad (3)$$

where  $N = 2^n - 1$  and all elements of the set  $\phi = \{\alpha^l | l = 1, 2, \dots, N - K_1\}$  are the roots of  $\mathbf{g}_1(x)$ . Furthermore, the systematic codeword polynomial  $\mathbf{c}_1(x)$  of  $RS_1$  can be obtained from  $\mathbf{g}_1(x)$  as below:

$$\mathbf{c}_1(x) = x^{N-K_1}\mathbf{m}_1(x)(1 + 1/\mathbf{g}_1(x)) \quad (4)$$

where  $\mathbf{m}_1(x) = m_0^{(1)} + m_1^{(1)}x + m_2^{(1)}x^2 + \cdots + m_{K_1-1}^{(1)}x^{K_1-1}$  is the polynomial of information symbols vector  $\mathbf{m}_1$  with coefficient  $m_i^{(1)} (i \in [0 : K_1 - 1]) \in GF(2^n)$ . Then, the codeword  $\mathbf{c}_1 = [c_0^{(1)}, c_1^{(1)}, \dots, c_{N-1}^{(1)}] (c_i^{(1)} \in GF(2^n), i \in [0 : N - 1])$  passes to the buffer that divides  $\mathbf{c}_1$  into short sequence  $\mathbf{c}_1(t)$  of length  $N_T = 3$  and  $t = [0 : N/N_T - 1]$ . Through the symbol splitter, each symbol contained in  $\mathbf{c}_1(t)$  is split out one by one denoted as  $c_{3t}^{(1)}, c_{3t+1}^{(1)}$  and  $c_{3t+2}^{(1)}$ , respectively. Each symbol in  $GF(2^n)$  corresponds to a binary vector  $\mathbf{b}^{(1)} = [b_0^{(1)}, b_1^{(1)}, \dots, b_{l-1}^{(1)}]$  of length  $l = \log_2 M$ ,  $M = 16$  or  $64$ . Therefore,  $c_{3t+a}^{(1)} (a \in [0 : 2])$  is mapped into a binary message vector  $\mathbf{b}_{q(3t+a)}^{(1)} = [b_{q(3t+a),0}^{(1)}, b_{q(3t+a),1}^{(1)}, \dots, b_{q(3t+a),l-1}^{(1)}]$  through  $M$ -ary symbols to bits block. Let  $q_{3t+a} = 1 + \sum_{m=0}^{l-1} 2^m b_{q(3t+a),m}^{(1)}$  that is the index of  $\mathbf{b}_{q(3t+a)}^{(1)}$ . Note that the Buffer, Symbol Splitter, and  $M$ -ary Symbols to Bits

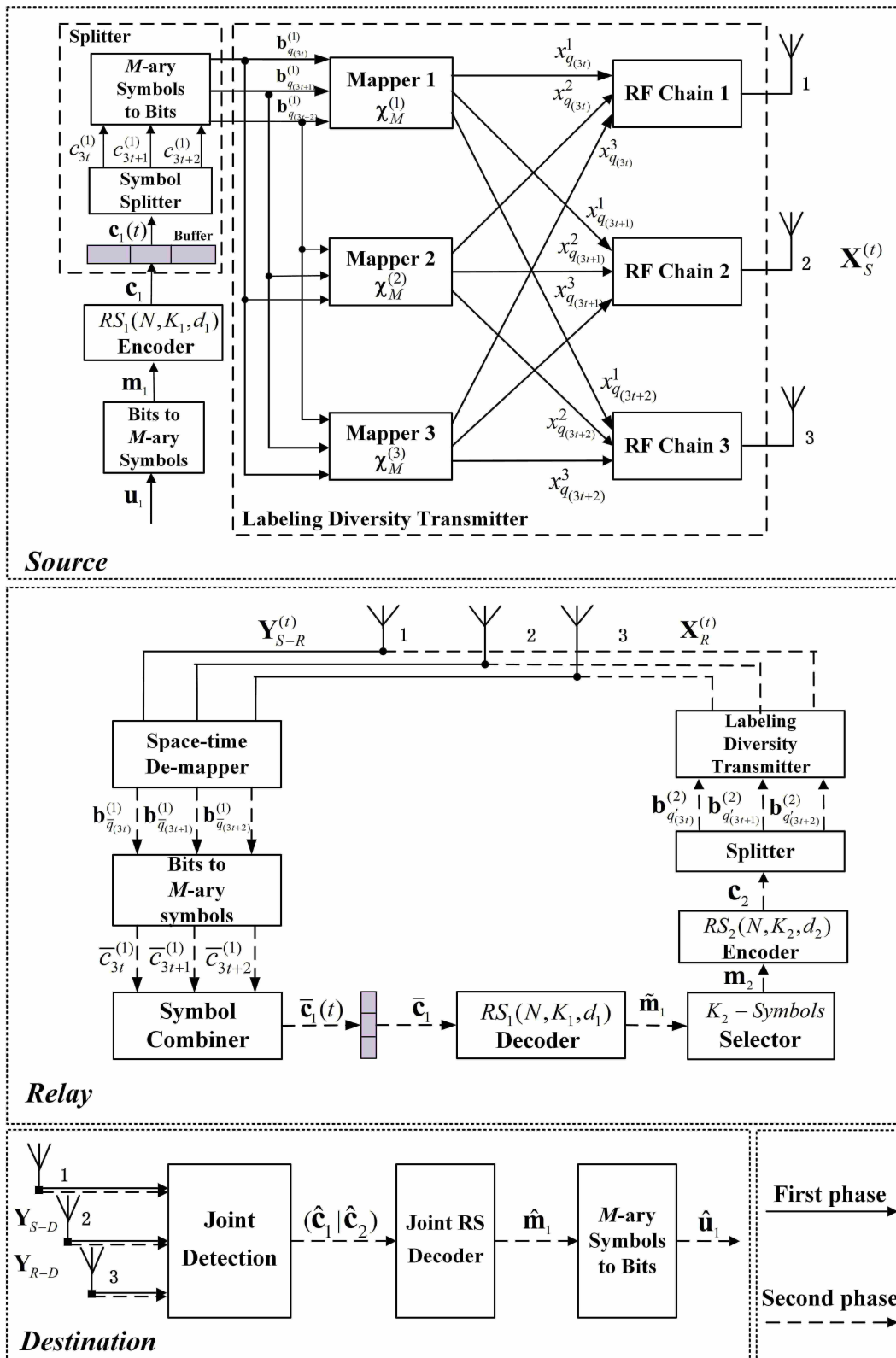


Fig. 2. The diagram of the proposed DRSCC-LD scheme for  $3 \times 3$  WLAN network.

blocks compose the Splitter block shown in Fig. 2. Subsequently, the bit stream  $\mathbf{b}_{q(3t+a)}^{(1)}$  is fed into three different mappers: mapper 1  $\chi_M^{(1)}$ , mapper 2  $\chi_M^{(2)}$  and mapper 3  $\chi_M^{(3)}$ . Moreover,  $\chi_M^{(k)}(\mathbf{b}_{q(3t+a)}^{(1)})$  maps  $\mathbf{b}_{q(3t+a)}^{(1)}$  into  $M$ -QAM constellation points in the complex plane, yielding  $x_{q(3t+a)}^k = \chi_M^{(k)}(\mathbf{b}_{q(3t+a)}^{(1)})$ ,  $k \in [1 : 3]$ ,  $a \in [0 : 2]$ , and  $t \in [0 : N/N_T - 1]$ . In the proposed DRSCC-LD scheme, the first mapper  $\chi_M^{(1)}$  employs Gray mapper, while the mappers  $\chi_M^{(2)}$  and  $\chi_M^{(3)}$  are designed with the purpose of optimizing the minimal product distance [23]. Krasicki et al [7] have proposed an optimal mapper that is applied in the mapper 2  $\chi_M^{(2)}$ . The design of mapper 3  $\chi_M^{(3)}$  is based on symmetrically swapping various amplitude [24]. For concrete demonstration, Table 1 depicts three different mapping results of 16-QAM in LD scheme for each symbol over  $\text{GF}(2^4)$ . In Tab. 1,  $\gamma$  is a primitive element of  $\text{GF}(2^4)$  and  $\gamma^i$  ( $i = 0, 1, \dots, 14$ ) including  $\gamma^{-\infty} = 0$  comprises all of elements of  $\text{GF}(2^4)$ . Besides, 64-QAM labeling mappers are illustrated in Fig. 3. Assume that the average signal energy is unity. After mapping the binary vectors, the signals are further sent to the RF module. Note that three different mappers and the corresponding RF chains make up the LD transmitter. The antennas 1, 2 and 3 simultaneously transmit  $x_{q(3t)}^1, x_{q(3t+1)}^1$  and  $x_{q(3t+2)}^1$ , respectively, in the 1<sup>st</sup> time slot,  $x_{q(3t)}^2, x_{q(3t+1)}^2$  and  $x_{q(3t+2)}^2$ , respectively, in the 2<sup>nd</sup> time slot and  $x_{q(3t)}^3, x_{q(3t+1)}^3$  and  $x_{q(3t+2)}^3$ , respectively, in the 3<sup>rd</sup> time slot. Let the transmitted space-time LD codeword vector at the source be defined as  $\mathbf{x}_S^{k,t} = [x_{q(3t)}^k, x_{q(3t+1)}^k, x_{q(3t+2)}^k]^T$ ,  $k \in [1 : 3]$ ,  $t \in [0 : N/N_T - 1]$ , where  $[\cdot]^T$  denotes the transpose of a matrix. Hence, the space-time codeword  $\mathbf{X}_S^{(t)}$  generated at each  $t$  is determined at the source as follows:

$$\mathbf{X}_S^{(t)} = [\mathbf{x}_S^{1,t}, \mathbf{x}_S^{2,t}, \mathbf{x}_S^{3,t}] = \begin{bmatrix} x_{q(3t)}^1 & x_{q(3t)}^2 & x_{q(3t)}^3 \\ x_{q(3t+1)}^1 & x_{q(3t+1)}^2 & x_{q(3t+1)}^3 \\ x_{q(3t+2)}^1 & x_{q(3t+2)}^2 & x_{q(3t+2)}^3 \end{bmatrix}. \quad (5)$$

In (5), the three rows correspond to the modulated symbols transmitted by three antennas, i.e., antennas 1, 2, and 3, respectively. Similarly, the three columns correspond to the symbols transmitted in the three-time slots, i.e., the 1<sup>st</sup>, 2<sup>nd</sup>, and 3<sup>rd</sup> time slot, respectively, which explains the space-time LD model. Assume that the channels for S-R and S-D link are Rayleigh frequency-flat fast fading channels, i.e., for each  $t$ , the channel  $\mathbf{H}_{S-R}^{k,t}$  and  $\mathbf{H}_{S-D}^{k,t}$  stay constant through each time slot  $k$  and have independent values in time slots 1, 2, and 3, respectively. More specifically, in the general case,  $\mathbf{H}_{S-R}^{1,t} \neq \mathbf{H}_{S-R}^{2,t} \neq \mathbf{H}_{S-R}^{3,t}$  and  $\mathbf{H}_{S-D}^{1,t} \neq \mathbf{H}_{S-D}^{2,t} \neq \mathbf{H}_{S-D}^{3,t}$ . Then, the received signal vectors for each time slot  $k$  ( $k \in [1 : 3]$ ) at the relay and destination are given by:

$$\mathbf{y}_{S-R}^{k,t} = \mathbf{H}_{S-R}^{k,t} \mathbf{x}_S^{k,t} + \mathbf{n}_{S-R}^{k,t}, \quad (6.a)$$

$$\mathbf{y}_{S-D}^{k,t} = \mathbf{H}_{S-D}^{k,t} \mathbf{x}_S^{k,t} + \mathbf{n}_{S-D}^{k,t} \quad (6.b)$$

where  $\mathbf{y}_{S-R}^{k,t} \in \mathbb{C}^{N_R \times 1}$  and  $\mathbf{y}_{S-D}^{k,t} \in \mathbb{C}^{N_R \times 1}$  are the  $k$ -th received signal vectors from the S-R link and S-D link, respectively.  $\mathbf{H}_{S-R}^{k,t} = [\mathbf{h}_{S-R,1}^{k,t}, \mathbf{h}_{S-R,2}^{k,t}, \mathbf{h}_{S-R,3}^{k,t}]$  and  $\mathbf{H}_{S-D}^{k,t} = [\mathbf{h}_{S-D,1}^{k,t}, \mathbf{h}_{S-D,2}^{k,t}, \mathbf{h}_{S-D,3}^{k,t}]$ , where  $\mathbf{h}_{S-R,i}^{k,t} \in \mathbb{C}^{N_R \times 1}$  and  $\mathbf{h}_{S-D,i}^{k,t} \in \mathbb{C}^{N_R \times 1}$  are the  $k$ -th fading channel vectors for the  $i$ -th transmit antenna from source to relay and destination, respectively. Moreover, each entry of  $\mathbf{h}_{S-R,i}^{k,t}$  and  $\mathbf{h}_{S-D,i}^{k,t}$  are i.i.d complex RVs defined same as that of  $\mathbf{H}_{S-R}$  and  $\mathbf{H}_{S-D}$ , respectively, mentioned in Sec. 2. Also,  $\mathbf{n}_{S-R}^{k,t} \in \mathbb{C}^{N_R \times 1}$  and  $\mathbf{n}_{S-D}^{k,t} \in \mathbb{C}^{N_R \times 1}$  are AWGN vectors whose element are also i.i.d complex RVs according to  $CN(0, \sigma^2)$ . Corresponding to the discussion in Sec. 2, the received signal matrix  $\mathbf{Y}_{S-R}^{(t)} = [\mathbf{y}_{S-R}^{1,t}, \mathbf{y}_{S-R}^{2,t}, \mathbf{y}_{S-R}^{3,t}]$  and  $\mathbf{Y}_{S-D}^{(t)} = [\mathbf{y}_{S-D}^{1,t}, \mathbf{y}_{S-D}^{2,t}, \mathbf{y}_{S-D}^{3,t}]$  are obtained at the relay and destination, respectively.

Field element	Binary vector	$\chi_{16}^{(1)}$	$\chi_{16}^{(2)}$	$\chi_{16}^{(3)}$
0	[0000]	$-3+j3$	$-1-j$	$1-j$
1	[1000]	$3+j3$	$1-j$	$-1-j$
$\gamma$	[0100]	$-1+j3$	$3+j$	$-3-j$
$\gamma^2$	[0010]	$-3-j3$	$-1+j$	$1+j$
$\gamma^3$	[0001]	$-3+j$	$-1+3j$	$-1+3j$
$\gamma^4$	[1100]	$1+j3$	$-3+j$	$3-j$
$\gamma^5$	[0110]	$-1-j3$	$3-j$	$-3+j$
$\gamma^6$	[0011]	$-3-j$	$-1-3j$	$-1-3j$
$\gamma^7$	[1101]	$1+j$	$-3-3j$	$-3-3j$
$\gamma^8$	[1010]	$3-j3$	$1+j$	$-1+j$
$\gamma^9$	[0101]	$-1+j3$	$3-3j$	$3-3j$
$\gamma^{10}$	[1110]	$1-3j$	$-3-j$	$3+j$
$\gamma^{11}$	[0111]	$-1-j$	$3+3j$	$3+3j$
$\gamma^{12}$	[1111]	$1-j3$	$-3+3j$	$-3+3j$
$\gamma^{13}$	[1011]	$3-j$	$1-3j$	$1-3j$
$\gamma^{14}$	[1001]	$3+j$	$1+3j$	$1+3j$

Tab. 1. Three different mapping results of each symbol over  $\text{GF}(2^4)$ .

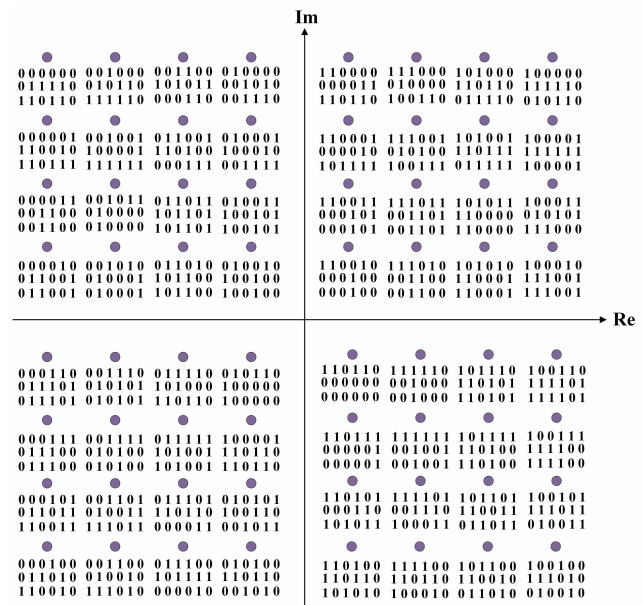


Fig. 3. 64-QAM mappers: mapper 1  $\chi_M^{(1)}$ , mapper 2  $\chi_M^{(2)}$  [7] and mapper 3  $\chi_M^{(3)}$  [24].

Simultaneously,  $\mathbf{Y}_{S-R}^{(t)}$  received at the relay passes to the 'Space-time de-mapper' block which first performs ML or proposed *RC-VSS* detection for the index  $q_{(3t+a)}$ ,  $a \in [0 : 2]$  of the binary vector  $\mathbf{b}_{q_{(3t+a)}}^{(1)}$  which will be presented in detail in Sec. 5, then demodulates the detected index  $\tilde{q}_{(3t+a)}$  to the binary sequence  $\mathbf{b}_{\tilde{q}_{(3t+a)}}^{(1)}$ .

In the second phase, the demodulated signal vector  $\mathbf{b}_{\tilde{q}_{(3t+a)}}^{(1)}$ ,  $a \in [0 : 2], t \in [0 : N/N_T - 1]$  is propagated to the bits to '*M*-ary symbols' block to recover symbols  $\tilde{c}_{3t+a}^{(1)}$  over  $\text{GF}(2^n)$  and then passes to symbol combiner block to form a short vector  $\tilde{\mathbf{c}}_1(t) = [\tilde{c}_{3t}^{(1)}, \tilde{c}_{3t+1}^{(1)}, \tilde{c}_{3t+2}^{(1)}]$ , and subsequently, enters the buffer to obtain the whole detected *RS*<sub>1</sub> code  $\tilde{\mathbf{c}}_1$  which is further decoded to get estimated message symbol sequence  $\tilde{\mathbf{m}}_1$ . Following that, the relay chooses exactly  $K_2$  information symbols from  $\tilde{\mathbf{m}}_1$  by an optimized search approach [19] as a message sequence  $\mathbf{m}_2$  which is then encoded by *RS*<sub>2</sub>( $N, K_2, d_2$ ) to obtain the systematic codeword  $\mathbf{c}_2$  of length  $N$  with the free distance  $d_2 = N - K_2 + 1$ . Moreover, the generator polynomial  $\mathbf{g}_2(x)$  of *RS*<sub>2</sub> with  $N - K_2$  consecutive power of a primitive element  $\beta \in \text{GF}(2^n)$  and the systematic codeword polynomial  $\mathbf{c}_2(x)$  acquired from  $\mathbf{g}_2(x)$  are given as:

$$\mathbf{g}_2(x) = (x - \beta)(x - \beta^2) \cdots (x - \beta^{N-K_2}), \quad (7)$$

$$\mathbf{c}_2(x) = x^{N-K_2} \mathbf{m}_2(x) (1 + 1/\mathbf{g}_2(x)) \quad (8)$$

where  $\mathbf{m}_2(x) = m_0^{(2)} + m_1^{(2)}x + m_2^{(2)}x^2 + \cdots + m_{K_2-1}^{(2)}x^{K_2-1}$  with each coefficient  $m_i^{(2)}$  ( $i \in [0 : K_2 - 1]$ )  $\in \text{GF}(2^n)$ . Then, the re-encoded information symbol vector  $\mathbf{c}_2 = [c_0^{(2)}, c_1^{(2)}, \dots, c_{N-1}^{(2)}]$  ( $c_i^{(2)} \in \text{GF}(2^n), i \in [0 : N - 1]$ ) also passes to the splitter block similar as the process in the first phase to obtain the corresponding binary vector  $\mathbf{b}_{q_{(3t+a)}}^{(2)} = [b_{q_{(3t+a)},0}^{(2)}, b_{q_{(3t+a)},1}^{(2)}, \dots, b_{q_{(3t+a)},l-1}^{(2)}]$ , where  $q_{(3t+a)} = 1 + \sum_{m=0}^{l-1} 2^m b_{q_{(3t+a)},m}^{(1)}$  is the index of  $\mathbf{b}_{q_{(3t+a)}}^{(2)}$ ,  $a \in [0 : 2], t \in [0 : N/N_T - 1]$ . Subsequently, three bit-streams are transmitted to the LD transmitter block employing three mappers identical to the process in the first phrase that generates the signal matrix  $\mathbf{X}_R^{(t)} = [\mathbf{x}_R^{1,t}, \mathbf{x}_R^{2,t}, \mathbf{x}_R^{3,t}]$  at the relay, where  $\mathbf{x}_R^{k,t} = [x_{q_{(3t)}}^k, x_{q_{(3t+1)}}^k, x_{q_{(3t+2)}}^k]^T$ ,  $k \in [1 : 3]$ . Each entry of  $\mathbf{x}_R^{k,t}$  presents the transmitted signal at the  $k$ -th time slot. Finally,  $\mathbf{X}_R^{(t)}$  is transmitted to the destination and the received signal  $\mathbf{y}_{R-D}^{k,t}$  from relay to destination is modeled as:

$$\mathbf{y}_{R-D}^{k,t} = \mathbf{H}_{R-D}^{k,t} \mathbf{x}_R^{k,t} + \mathbf{n}_{R-D}^{k,t} \quad (9)$$

where  $\mathbf{H}_{R-D}^{k,t}$  and  $\mathbf{n}_{R-D}^{k,t}$  are Rayleigh frequency-flat fast fading channel and AWGN matrices, respectively, and similarly defined as  $\mathbf{H}_{S-R}^{k,t}$  and  $\mathbf{n}_{S-R}^{k,t}$  in (5.b). Similarly, the signal matrix  $\mathbf{Y}_{R-D}^{(t)} = [\mathbf{y}_{R-D}^{1,t}, \mathbf{y}_{R-D}^{2,t}, \mathbf{y}_{R-D}^{3,t}]$  is acquired in the second phase at the destination.

Then, the received whole signal matrices  $\mathbf{Y}_{S-D}^{(t)}$  and  $\mathbf{Y}_{R-D}^{(t)}$  for  $t \in [0 : N/N_T - 1]$  are demodulated by 'Joint Detection' block to obtain jointly recovered non-binary information vector  $(\hat{\mathbf{c}}_1 | \hat{\mathbf{c}}_2)$ . Subsequently,  $(\hat{\mathbf{c}}_1 | \hat{\mathbf{c}}_2)$  is transmitted to the 'Joint RS Decoder' module to acquire the estimated message sequence  $\hat{\mathbf{m}}_1$  of length  $K_1$  with the assist of critical SNR. Sections 5 and 6 will elaborate the two key modules. Finally, '*M*-ary Symbols to Bits' block converts  $\hat{\mathbf{m}}_1$  to estimated binary sequence  $\hat{\mathbf{u}}_1$ .

## 4. Theoretical Performance Analysis

In this section, we derive the error performance bound of the proposed DRSCC-LD scheme. Firstly, the theoretical ABEP of non-cooperative RS coded LD scheme is formulated employing the union bound. Then, we extend the asymptotic performance analysis to the coded cooperative communication scheme.

### 4.1 The Theoretical ABEP Derivation of Non-Cooperative RS Coded LD Scheme

Ayanda et al. [24] have studied the performance analysis of uncoded space-time labeling diversity (USTLD) scheme with three transmitter antennas where only one triad of the symbol is incorrectly detected at the high SNR. For the RS coded  $3 \times 3$  space-time LD scheme, we first consider the S-D link and follow the same assumption that  $x_{q_{(3t)}}^k$  ( $t \in [0 : N/N_T - 1], k \in [1 : 3]$ ) is detected with errors while  $x_{q_{(3t+1)}}^k$  and  $x_{q_{(3t+2)}}^k$  are correctly detected. Therefore, (6.b) can be equivalently modeled as:

$$\mathbf{y}_{S-D}^{k,t} = \mathbf{h}_{S-D,1}^{k,t} x_{q_{(3t)}}^k + \mathbf{n}_{S-D}^{k,t}. \quad (10)$$

Since each symbol of RS code over  $\text{GF}(2^n)$  corresponds to a constellation point, the core idea of deriving the average bit error probability (ABEP) is first to determine the average error probability of each symbol  $P_s$  and then obtain the ABEP of point-to-point RS coded LD scheme. Firstly, the union bound of  $P_s$  is defined as [24]:

$$P_s \geq \frac{N_T}{MN} \sum_{t=0}^{N/N_T-1} \sum_{q_{(3t)}=1}^M \sum_{\hat{q}_{(3t)} \neq q_{(3t)}}^M P(\mathbf{X}_S^{(t)} \rightarrow \hat{\mathbf{X}}_S^{(t)}) \quad (11)$$

where  $P(\mathbf{X}_S^{(t)} \rightarrow \hat{\mathbf{X}}_S^{(t)})$  is the pairwise error probability (PEP) between the transmitted part symbol matrix  $\mathbf{X}_S^{(t)}$  and the received part symbol matrix  $\hat{\mathbf{X}}_S^{(t)}$ . The detailed derivation procedure of the PEP over Rayleigh frequency-flat fast fading channel is given in [25], and similarly, we obtain:

$$P(\mathbf{X}_S^{(t)} \rightarrow \hat{\mathbf{X}}_S^{(t)}) = \frac{1}{2n} \left[ \frac{1}{2} \prod_{k=1}^3 \left( 1 + \frac{\varepsilon_1 R_1 d_1}{12} \rho_t^k \right)^{-N_R} + \sum_{j=1}^{\tau-1} \prod_{k=1}^3 \left( 1 + \frac{\varepsilon_1 R_1 d_1}{12 \sin^2(\frac{j\pi}{\tau})} \rho_t^k \right)^{-N_R} \right] \quad (12)$$

where  $\varepsilon_1$  denotes the average SNR of the S-D link,  $\tau$  is a constant greater than 10, and  $R_1 = K_1/N$  is the code rate of  $RS_1(N, K_1, d_1)$ . Moreover,  $\rho_t^k = |\omega_t^k|^2 \|\mathbf{h}_{S-D,1}^{1,t}\|_F^2$ , where  $\omega_t^k = x_{q(3t)}^k - \hat{x}_{q(3t)}^k$  and  $\|\cdot\|_F$  represents the Frobenius norm. Therefore,  $P_s$  is acquired by substituting (12) to the (11) and the average bit error probability ABEP of the non-cooperative RS coded LD scheme for S-D link may be defined as [20]:

$$ABEP \geq \frac{1}{\log_2 M} \sum_{\xi=\mu_1+1}^N \xi \binom{N}{\xi} (P_s)^\xi (1-P_s)^{N-\xi} \quad (13)$$

where  $\mu_1 = (N-K_1)/2$  which represents the number of error symbols that  $RS_1$  code can correct.

## 4.2 Asymptotic Performance Analysis of DRSCC-LD Scheme

For the coded-cooperative LD scheme, the PEP in (12) will become the joint PEP in reference to the S-D and R-D links, i.e.,  $P(\mathbf{X}_S^{(t)} \rightarrow \hat{\mathbf{X}}_S^{(t)})$  and  $P(\mathbf{X}_R^{(t)} \rightarrow \hat{\mathbf{X}}_R^{(t)})$ , respectively. Mathematically [16],

$$P(\mathbf{X}^{(t)} \rightarrow \hat{\mathbf{X}}^{(t)}) = P(\mathbf{X}_S^{(t)} \rightarrow \hat{\mathbf{X}}_S^{(t)})P(\mathbf{X}_R^{(t)} \rightarrow \hat{\mathbf{X}}_R^{(t)}). \quad (14)$$

As the relay R and source S are both viewed as transmitters, the derivation for the R-D link is the same. Therefore, the joint PEP can be further written as:

$$P(\mathbf{X}^{(t)} \rightarrow \hat{\mathbf{X}}^{(t)}) = \frac{1}{2n} \left[ \frac{1}{2} \prod_{k=1}^3 \left( 1 + \frac{\varepsilon_1 R_1 d_1}{12} \rho_t^k \right)^{-N_R} + \sum_{j=1}^{\tau-1} \prod_{k=1}^3 \left( 1 + \frac{\varepsilon_1 R_1 d_1}{12 \sin^2(\frac{j\pi}{2\tau})} \rho_t^k \right)^{-N_R} \right] \times \frac{1}{2n} \left[ \frac{1}{2} \prod_{k=1}^3 \left( 1 + \frac{\varepsilon_2 R_2 d_2}{12} \tilde{\rho}_t^k \right)^{-N_R} + \sum_{j=1}^{\tau-1} \prod_{k=1}^3 \left( 1 + \frac{\varepsilon_2 R_2 d_2}{12 \sin^2(\frac{j\pi}{2\tau})} \tilde{\rho}_t^k \right)^{-N_R} \right] \quad (15)$$

where  $\varepsilon_2$  represents the total average SNR of the R-D link,  $R_2 = K_2/N$ , and  $\tilde{\rho}_t^k = |\tilde{\omega}_t^k|^2 \|\mathbf{h}_{R-D,1}^{1,t}\|_F^2$ ,  $\tilde{\omega}_t^k = x_{q(3t)}^k - \hat{x}_{q(3t)}^k$ .

Hence, the ABEP of the DRSCC-LD scheme can be determined by replacing  $P(\mathbf{X}^{(t)} \rightarrow \hat{\mathbf{X}}^{(t)})$  in (15) into (11) and (13) in succession. Note that  $RS_2$  can correct  $\mu_2 = (N-K_2)/2$  errors, where  $\mu_2 \geq \mu_1$ . Therefore, the variable  $\xi$  goes from  $\mu_2 + 1$  to  $N$  in (13). The derived theoretical bound exhibits a tight match with simulation results in Sec. 7 at the high SNR which verifies the rationality of the proposed DRSCC-LD scheme.

## 5. Novel Joint Detection Scheme

This section introduces the 'Space-time De-mapper block' which employs the optimal ML detection scheme from the S-D link that is also applicable to the R-D link. In the proposed scheme,  $M$ -QAM ( $M = 16$  and  $64$ ) are employed in the LD where the binary vector of length  $n$  ( $n = 4$  for 16-QAM

and  $n = 6$  for 64-QAM) is mapped in the constellation. Note that each symbol of the RS code is over  $GF(2^n)$  which may directly correspond to the constellation signal. Moreover, the code length  $N$  is restricted by  $N = 2^n - 1$ , which implies that  $N = 15$  and  $63$  are determined to be compatible with the modulation schemes. Therefore, ML detection is applied for the  $M$ -QAM modulation with short-to-medium-length RS codes. However, due to the high complexity of ML detection, a  $RC$ -VSS detection algorithm is proposed subsequently, which can provide a novel idea for lowering the detection complexity of other space-time coded modulation schemes. To enhance the diversity gain, the two signals received at the destination are further jointly detected based on the proposed  $RC$ -VSS algorithm.

## 5.1 Optimal ML Detection Scheme

Suppose that the receiver has perfect channel state information (CSI). To estimate the transmitted symbols, minimize the ML formulation provided by:

$$\left[ \hat{q}_{(3t)}, \hat{q}_{(3t+1)}, \hat{q}_{(3t+2)} \right] = \arg \min_{\substack{q_{(3t+a)} \in [1:M], \\ a \in [0:2]}} \left( \sum_{k=1}^3 \|\mathbf{y}_{S-D}^{k,t} - \mathbf{H}_{S-D}^{k,t} \mathbf{x}_S^{k,t}\|_F^2 \right), t \in [0 : N/N_T - 1]. \quad (16)$$

Trivially, the complexity of ML detection is proportional to  $O(M^3)$  which is quite high in the case of higher-order modulation. To make the proposed scheme more practical, the  $RC$ -VSS algorithm is presented in the next subsection to reduce the complexity of the detection of the DRSCC-LD scheme.

## 5.2 Proposed RC-VSS algorithm

The proposed  $RC$ -VSS detection algorithm is based on the orthogonal projection approach [25]. The procedure is illustrated in Algorithm 1 using the signal in (6.b) received at the destination in the first phase as an example. The algorithm is completed through four stages. The signal subset  $\tilde{\mathcal{X}}_M^{(i)}, i \in [1 : 3]$  varies depending on the selection of the length  $L$  ( $1 \leq L \leq M$ ) of the promising index set  $\Omega_{t,a}^L, t \in [0 : N/N_T - 1], a \in [0 : 2]$ . Based on  $\Omega_{t,a}^L$ , the received signal is detected with complexity proportional to  $O(L^3)$ .

---

### Algorithm 1. Proposed $RC$ -VSS algorithm

---

**Input:**  $N, N_T, N_R, M, \mathbf{y}_{S-D}^{k,t}, \mathbf{H}_{S-D}^{k,t}, \mathbf{x}_S^{k,t}$

**Output:** The estimated index  $\hat{q}_{(3t)}, \hat{q}_{(3t+1)}$  and  $\hat{q}_{(3t+2)}$

**for**  $t = 0 : N/N_T - 1$  **do**

**First stage:** Determine the projection matrices  $\Delta_i^{k,t}$  and the projection spaces  $\gamma_{i,q(3t+a)}^{k,t}$ .

**for**  $k = 1 : 3$  **do**

**for**  $i = 1 : 3$  **do**

(1)  $\mathbf{H}_{S-D,i}^{k,t} = \mathbf{H}_{S-D}^{k,t} \setminus \mathbf{h}_{S-D,i}^{k,t}$  (Remove the  $i$ -th column of  $\mathbf{H}_{S-D}^{k,t}$ );

(2)  $\mathbf{Z}_i^{k,t} = \mathbf{H}_{S-D,i}^{k,t} ((\mathbf{H}_{S-D,i}^{k,t})^H \mathbf{H}_{S-D,i}^{k,t})^{-1} (\mathbf{H}_{S-D,i}^{k,t})^H$ ;

(3)  $\Delta_i^{k,t} = \mathbf{I}_{N_R} - \mathbf{Z}_i^{k,t}$ ,  $\mathbf{I}_{N_R}$  is a  $N_R \times N_R$  identity matrix.

**for**  $a = 0 : 2$  **do**

$$\gamma_{i,q(3t+a)}^{k,t} = \mathbf{y}_{S-D}^{k,t} - \mathbf{h}_{S-D,i}^{k,t} \mathbf{x}_{q(3t+a)}^k$$

**end for**

**end for**

**Second stage:** Calculate the metric sets  $\Lambda_{q(3t+a)}^t$  based on  $\Delta_i^{k,t}$  and  $\gamma_{i,q(3t+a)}^{k,t}$ .

**for**  $i = 1 : 3$  **do**

**for**  $a = 0 : 2$  **do**

$$\Lambda_{q(3t+a)}^t = \sum_{k=1}^3 \|\Delta_i^{k,t} (\gamma_{i,q(3t+a)}^{k,t})\|_F^2, q(3t+a) \in [1 : M]$$

**end for**

**end for**

**Third stage:** Determine the length  $L$  of the index sets  $\Omega_{t,a}^L$  corresponding to a variable signal subset  $\tilde{\chi}_M^{(i)}$ .

**for**  $a = 0 : 2$  **do**

(1) Sort  $\Lambda_{q(3t+a)}^t$  in ascending order as :

$$\Lambda_{q(3t+a)}^t = \{e_{q(3t+a),1}, e_{q(3t+a),2}, \dots, e_{q(3t+a),M}\};$$

(2) Select the index  $q(3t+a),i$  ( $1 \leq i \leq L, 1 \leq L \leq M$ ) of the first  $L$  items in the set  $\Lambda_{q(3t+a)}^t$ ;

(3) Determine the subset  $\Omega_{t,a}^L$

$$\Omega_{t,a}^L = \{q(3t+a),1, q(3t+a),2, \dots, q(3t+a),L\};$$

(4)  $\Omega_{t,a}^L \rightarrow \tilde{\chi}_M^{(i)}, i = a + 1$ .

**Fourth stage:** Joint detection based on  $\Omega_{t,a}^L$ .

$$\begin{aligned} & [\hat{q}(3t), \hat{q}(3t+1), \hat{q}(3t+2)] \\ & = \arg \min_{q(3t+a),i \in \Omega_{t,a}^L} (\sum_{k=1}^3 \|\mathbf{y}_{S-D}^{k,t} - \mathbf{h}_{S-D,i}^{k,t} \mathbf{x}_{q(3t+a),i}^k\|_F^2). \end{aligned}$$

**end for**

**end for**

### 5.3 Joint Detection of Two Signals at the Destination Based on RC-VSS Algorithm

This subsection elaborates the 'Joint Detection' block in Fig. 2 and its concrete block diagram is depicted in Fig. 4. Since the information sequence at the relay is selected from the source, the two signals received from the two transmitters are jointly detected to further obtain the diversity gain at the destination.

First, the received  $3 \times 3$  signal matrices  $\mathbf{Y}_{S-D}^{(t)}$  and  $\mathbf{Y}_{R-D}^{(t)}$  also pass to the 'Space-time De-mapper' block that can detect the part binary vectors  $\mathbf{b}_{\hat{q}(3t+a)}^{(1)}$  and  $\mathbf{b}_{\hat{q}(3t+a)}^{(2)}$  ( $a \in [0 : 2], t \in [0 : N/N_T - 1]$ ) based on RC-VSS algorithm, which are then combined to the whole information sequences  $\tilde{\mathbf{b}}_1 = (\mathbf{b}_{\hat{q}(0)}^{(1)}, \mathbf{b}_{\hat{q}(1)}^{(1)}, \dots, \mathbf{b}_{\hat{q}(N-1)}^{(1)})$  and  $\tilde{\mathbf{b}}_2 = (\mathbf{b}_{\hat{q}(0)}^{(2)}, \mathbf{b}_{\hat{q}(1)}^{(2)}, \dots, \mathbf{b}_{\hat{q}(N-1)}^{(2)})$  through the buffer, respectively. Subsequently, the binary message sequences  $\tilde{\mathbf{b}}_1$  and  $\tilde{\mathbf{b}}_2$  are converted to the symbol sequences  $\tilde{\mathbf{c}}_1$  and  $\tilde{\mathbf{c}}_2$ , respectively. Since  $RS_2$  with more consecutive roots performs better than  $RS_1$  at the high SNR, substitute the first  $K_2$  symbols of systematic codeword  $\tilde{\mathbf{c}}_2$  for the symbols of  $\tilde{\mathbf{c}}_1$  in the corresponding selection position

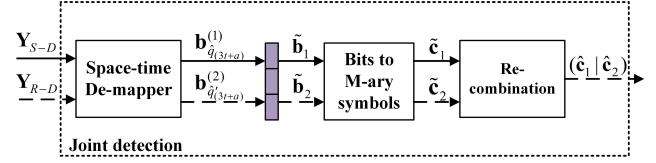


Fig. 4. The concrete diagram block of joint detection at the destination.

through 'Re-combination' block. Finally, the joint detected message sequence  $(\hat{\mathbf{c}}_1 | \hat{\mathbf{c}}_2)$  is obtained where one output  $\hat{\mathbf{c}}_1$  is reorganized by  $\tilde{\mathbf{c}}_1$  and  $\tilde{\mathbf{c}}_2$  and the other is  $\hat{\mathbf{c}}_2 = \tilde{\mathbf{c}}_2$ .

## 6. Critical SNR-Assisted Joint Decoding Scheme

The Euclidean decoding algorithm [26] is employed in the RS decoders which are utilized by the source and relay denoted as  $RS_1$  decoder and  $RS_2$  decoder, respectively. At the destination, we propose a novel critical SNR-assisted (CSA) joint decoding scheme that effectively incorporates the reliable message of the joint-detected information sequences  $(\hat{\mathbf{c}}_1 | \hat{\mathbf{c}}_2)$  to provide the coding gain to the DRSCC-LD scheme.

In our proposed DRSCC-LD scheme,  $RS_1(N, K_1, d_1)$  and  $RS_2(N, K_2, d_2)$  are considered at the source and relay, respectively, where  $K_1 \geq K_2$  and  $d_1 \leq d_2$ . Note that at the high SNR, a code with a larger free distance has a better capability of correcting errors, and vice versa. Therefore, the BER performance curves of  $RS_1$  and  $RS_2$  cross in the point-to-point communication, where the SNR corresponding to this intersection point is specified as the critical threshold value  $\delta$  employed in the joint decoding algorithm outlined in Algorithm 2.

#### Algorithm 2. Proposed CSA algorithm

**Input:** The joint detected sequence  $(\hat{\mathbf{c}}_1 | \hat{\mathbf{c}}_2)$

**Output:** The joint decoded message sequence  $\hat{\mathbf{m}}_1$

**First stage:** Input  $\hat{\mathbf{c}}_2$  of the joint detected sequence  $(\hat{\mathbf{c}}_1 | \hat{\mathbf{c}}_2)$  to the  $RS_2$  decoder to acquire the estimated message sequence  $\hat{\mathbf{m}}_2$  of length  $K_2$ .

**Second stage:** Determine the critical SNR threshold  $\delta$  by simulation.

**Third stage:** Joint decode assisted with  $\delta$  of the cross-point of the  $RS_1$  and  $RS_2$  non-cooperative coded scheme.

**if**  $SNR \geq \delta$  **then**

Substitute  $\hat{\mathbf{m}}_2$  for the  $K_2$  selected symbols of  $\hat{\mathbf{c}}_2$  corresponding to the selection pattern at the relay, then  $\hat{\mathbf{m}}_1$  is obtained;

**else**

$\hat{\mathbf{m}}_1 = \hat{\mathbf{c}}_1$

**end if**

**Fourth stage:** Transmit the joint-constructed sequence  $\hat{\mathbf{m}}_1$  into the the  $RS_1$  decoder, and get the final estimated message sequence  $\hat{\mathbf{m}}_1$ .

## 7. Simulation Results

The BER performance of the proposed DRSCC-LD scheme over the Rayleigh frequency-flat fading channel is illustrated in this section, where the channels for S-R, S-D, and R-D links have independent values in each time slot. The specific channel model is detailed in Sec. 3. Two different scenarios are considered in our proposed scheme where  $RS_1(15, 13, 3)$  and  $RS_2(15, 7, 9)$  generated by the irreducible polynomial  $1 + x + x^4$  over  $GF(2^4)$  are employed in the source and relay, respectively, for the first scenario and  $RS_1(63, 57, 7)$  and  $RS_2(63, 37, 27)$  constructed based on the polynomial  $1 + x + x^6$  over  $GF(2^6)$  are applied for the second scenario. Besides, the code rates for the first scenario are  $R_1 = 13/15$  and  $R_2 = 7/15$  and for the second scenario  $R_1 = 57/63$  and  $R_2 = 37/63$ , respectively. In the first scenario, each non-binary symbol of  $RS_1(15, 13, 3)$  and  $RS_2(15, 7, 9)$  are over  $GF(2^4)$  and can be denoted as a binary vector of length-4, which corresponds exactly to a complex signal symbol on the constellation of 16-QAM. Similarly, in the second scenario, each symbol over  $GF(2^6)$  corresponds to the point on the 64-QAM constellation. Therefore, 16-QAM and 64-QAM are considered in the modulation scheme for the feasibility of the proposed DRSCC-LD scheme in the two scenarios, respectively. Moreover, three different labels of the 16-QAM and 64-QAM shown in Tab. 1 and Fig. 3 are employed in the two scenarios, respectively. We define  $\Gamma_{S-R}$ ,  $\Gamma_{S-D}$  and  $\Gamma_{R-D}$  as the instantaneous SNR per bit for the S-R link, S-D link, and R-D link, respectively. Suppose that the R-D link has a 2 dB gain over the S-D link, i.e.,  $\Gamma_{R-D} = \Gamma_{S-D} + 2$  dB.

### 7.1 BER Performance of DRSCC-LD Scheme Under Different Selection Patterns at the Relay

Assume that the S-R link is ideal ( $\Gamma_{S-R} = \infty$ ). The proposed *RC-VSS* detection algorithm and *CSA* joint decoding algorithm are both employed in our proposed scheme.

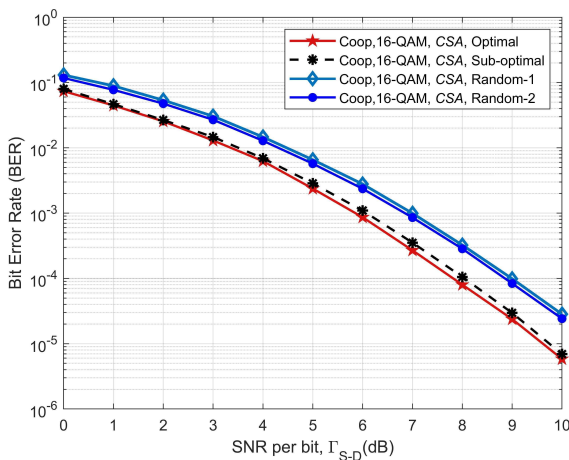


**Fig. 5.** The BER performance curves of the DRSCC-LD scheme for the first scenario under different selection patterns at the relay under  $\Gamma_{S-R} = \infty$ .

Besides, we also utilize a novel selection approach at the relay to obtain a better resultant code at the destination and further optimize the performance of DRSCC-LD. Table 2 exhibits the optimal, suboptimal selection patterns obtained by the approach described in [19] and the random patterns to compare. Figure 5 exhibits the BER performance curves for the first scenario where selecting the messages at the relay improves the overall performance of the proposed DRSCC-LD scheme by around 1.3 dB at the  $BER \approx 2.1 \times 10^{-5}$ . The simulation results also reveal that the performance of the DRSCC-LD scheme with the sub-optimal selection pattern is nearly identical to that with the optimal pattern at the low-to-medium SNR and slightly inferior at high SNR.

Similarly, the BER performance for the second scenario is plotted in Fig. 6 which demonstrates that the DRSCC-LD scheme under the sub-optimal selection pattern outperforms the proposed scheme under the random selections by about 0.6 dB at the  $BER \approx 8.6 \times 10^{-6}$ . Therefore, the sub-optimal selection pattern, which minimizes greatly the complexity of the search process, is adopted for the remainder performance analysis of the DRSCC-LD scheme for the second scenario.

### 7.2 BER Performance of DRSCC-LD Scheme Based on Variable Signal Subsets

For the proposed *RC-VSS* detection algorithm, the different signal subsets also influence the BER performance of the proposed DRSCC-LD scheme. As stated in Sec. 5.2, the difference in the index length  $L$  determines the various signal subsets. Therefore, we simulate with different  $L$  ( $1 \leq L \leq M$ ) values in order to find a more appropriate signal subset that balances the detection complexity and the BER performance of the DRSCC-LD scheme, where  $\Gamma_{S-R} = \infty$  and selection patterns are determined as discussed above. Figure 7 illustrates the BER performance of the DRSCC-LD schemes for the first scenario corresponding to five signal subsets. The results reveal that when  $L \leq M/2$ , the BER performance of the considered

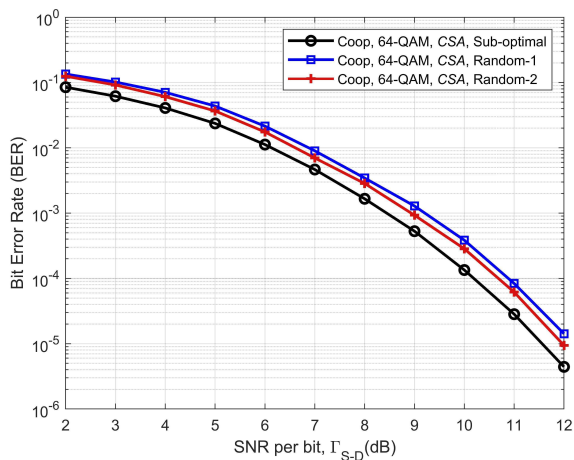


**Fig. 6.** The BER performance curves of the DRSCC-LD scheme for the second scenario under different selection patterns at the relay under  $\Gamma_{S-R} = \infty$ .

Scenario Series	RS codes	Selection approach	Selection pattern
1	Source: $RS_1(15, 13, 3)$ Relay: $RS_2(15, 7, 9)$	Optimal	[1 2 4 6 8 11 13]
		Sub-optimal	[1 2 3 5 7 10 12]
		Random 1	[1 2 3 4 5 11 12]
		Random 2	[1 2 3 5 7 10 12]
2	Source: $RS_1(63, 57, 7)$ Relay: $RS_2(63, 37, 27)$	Sub-optimal	[1 2 4 6 8 10 11 12 14 16 18 20 22 23 25 26 27 28 29 31 33 34 35 37 40 41 42 43 45 46 48 49 50 52 53 54 56]
		Random 1	[1 2 3 5 7 10 11 12 14 15 17 19 20 21 22 23 25 28 29 30 32 33 35 36 38 41 42 44 45 47 48 49 51 52 54 56 57]
		Random 2	[1 2 3 4 5 6 8 10 12 13 15 16 18 21 22 24 25 27 28 30 31 32 34 35 38 40 41 43 44 45 48 49 50 51 52 53 55]

Tab. 2. The optimal, sub-optimal and random selection patterns for two different scenarios.

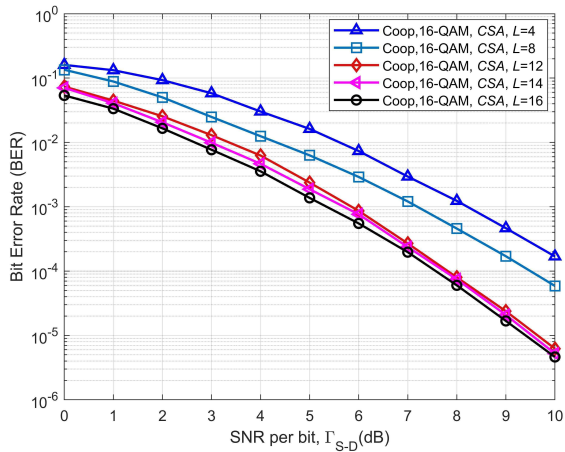


Fig. 7. The BER performance curves of the DRSCC-LD scheme for the first scenario with different signal subsets where  $\Gamma_{S-R} = \infty$  and selection pattern is optimal.

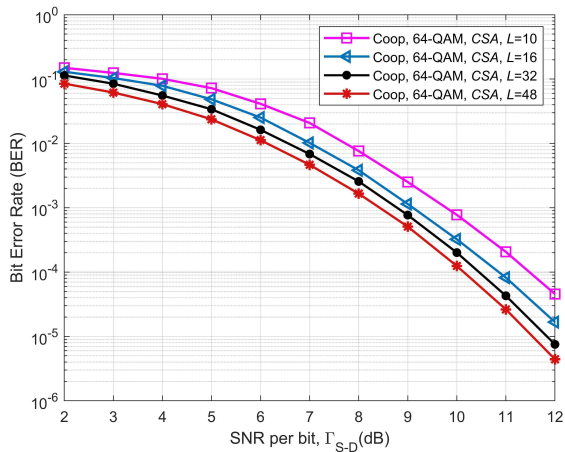


Fig. 8. The BER performance curves of the DRSCC-LD scheme for the second scenario with different signal subsets where  $\Gamma_{S-R} = \infty$  and selection pattern is sub-optimal.

DRSCC-LD scheme performs worse than that employed the optimal joint detection ( $L = M$ ) by around 2.4 ~ 2.7 dBs at the  $BER \approx 5.8 \times 10^{-6}$  while  $L > M/2$ , there is little difference in BER performance by margins of 0.1 ~ 0.3 dBs. Hence, we utilize  $L = 48$  to simplify the detection complexity of the proposed DRSCC-LD scheme in the second scenario. As illustrated in Fig. 8, the BER performance of the DRSCC-LD scheme with  $L = 48$  performs better than the corresponding scheme with other  $L$  values by a gain of approximately 0.5 ~ 1.7 dBs at the  $BER \approx 4.8 \times 10^{-5}$ .

### 7.3 BER Performance Comparisons of DRSCC-LD Schemes with CSA Joint Decoding Algorithm and Existing Decoding Schemes

To demonstrate the practicality of our proposed novel joint decoding algorithm, we compare the BER performance of the DRSCC-LD scheme utilizing the CSA algorithm to that of the scheme employing the existing algorithms where  $\Gamma_{S-R} = \infty$ . First, Figures 9 and 10 illustrate the process of finding the critical SNR threshold  $\delta$ , where  $\delta \approx 6.2$  dB for the first scenario and  $\delta \approx 9.6$  dB for the second scenario, respectively. In Fig. 11, the BER performance of the DRSCC-LD scheme employing the CSA algorithm outperforms the schemes using the other two existing decoding algorithms in [11], [20], i.e., naive and smart decoding algorithms for the first scenario by a gain of 0.8 dB and 0.3 dB at the  $BER \approx 1.7 \times 10^{-6}$ , respectively. Similarly, for the second scenario shown in Fig. 12, at the  $BER \approx 2.7 \times 10^{-5}$ , the DRSCC-LD scheme employing the CSA algorithm acquires 1.1 dB and 0.5 dB gain compared to the scheme using naive and smart algorithms, respectively. Therefore, the proposed CSA joint decoding algorithm may fully utilize the resources gained from the coded cooperation.

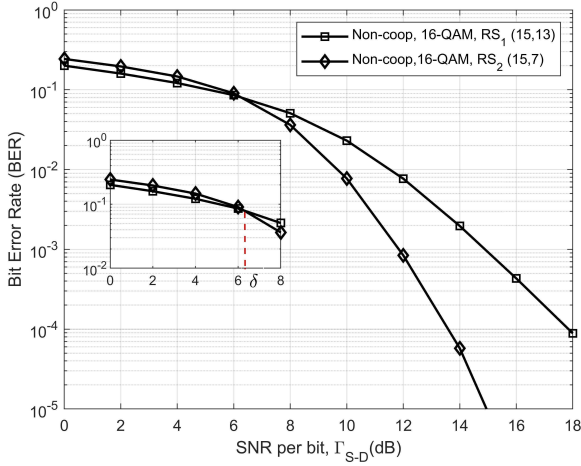


Fig. 9. The BER performance curves of  $RS_1(15, 13, 3)$  and  $RS_2(15, 7, 9)$  non-cooperative scheme to determine the critical SNR threshold  $\delta$ .

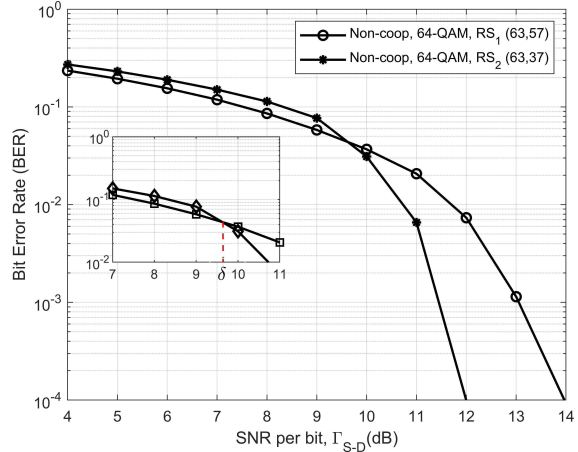


Fig. 10. The BER performance curves of  $RS_1(63, 57, 7)$  and  $RS_2(63, 37, 27)$  non-cooperative scheme to determine the critical SNR threshold  $\delta$ .

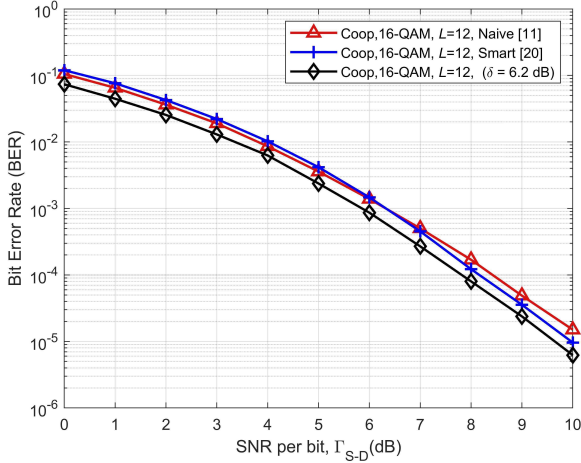


Fig. 11. The BER performance curves of the DRSCC-LD scheme employing CSA joint decoding algorithm and the scheme using other decoding algorithms for the first scenario.

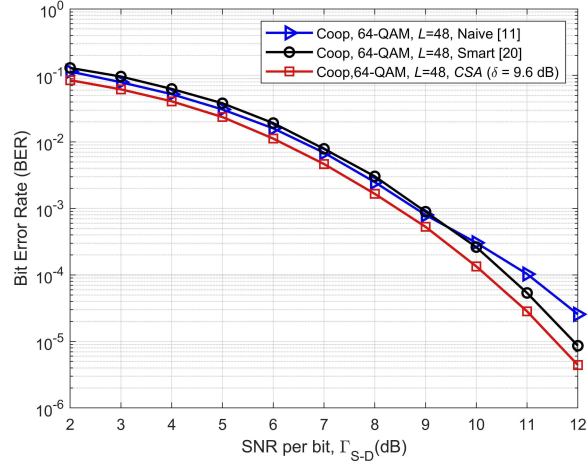


Fig. 12. The BER performance curves of the DRSCC-LD scheme employing CSA joint decoding algorithm and the scheme using other decoding algorithms for the second scenario.

### 7.4 BER Performance of DRSCC-LD Schemes Under Ideal and Non-Ideal S-R Channels

Practically, the ideal source-to-relay link ( $\Gamma_{S-R} = \infty$ ) stated above is not feasible. Hence, we compare the BER performance of the proposed DRSCC-LD scheme over a non-ideal link ( $\Gamma_{S-R} \neq \infty$ ) to the non-cooperative RS coded scheme with equal codes rate for two scenarios, respectively.

Illustrated in Figs. 13 and 14, the proposed DRSCC-LD scheme significantly outperforms the non-cooperative RS coded scheme in terms of BER performance on both the ideal ( $\Gamma_{S-R} = \infty$ ) and non-ideal ( $\Gamma_{S-R} \neq \infty$ ) S-R links by a gain of over 7 dB, generally, which indicates that the relay cooperation and LD technique have the impact on the

path diversity. In Fig. 13, when the source-to-relay channel condition is bad ( $\Gamma_{S-R} = 6$  dB), the BER performance of the DRSCC-LD scheme is poor at low SNRs and has an approximately 2.1 dB loss compared to the ideal link at  $BER \approx 7.1 \times 10^{-5}$  for the first scenario. Moreover, the performance of the proposed DRSCC-LD scheme with a better non-ideal S-R link ( $\Gamma_{S-R} = 26$  dB) has already been extremely similar to that with an ideal link ( $\Gamma_{S-R} = \infty$ ), with a gap of only 0.9 dB at  $BER \approx 2.2 \times 10^{-5}$ . The simulation results for the second scenario in Fig. 14 come to the same conclusion that the proposed DRSCC-LD performs poorly on the condition of  $\Gamma_{S-R} = 10$  dB, but considerably improves when  $\Gamma_{S-R} = 30$  dB. Note that the LD technique has significantly reduced the EF region occurred in [19] that further demonstrated the supremacy of the proposed DRSCC-LD scheme.

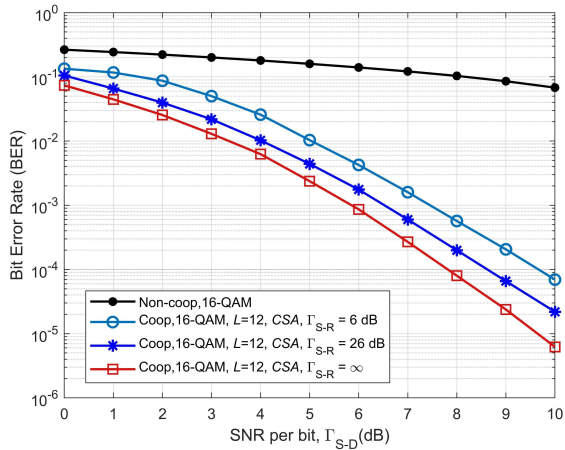


**Fig. 13.** The BER performance of the DRSCC-LD scheme under ideal and non-ideal S-R links compared to the performance of non-cooperative RS coded scheme for the first scenario.

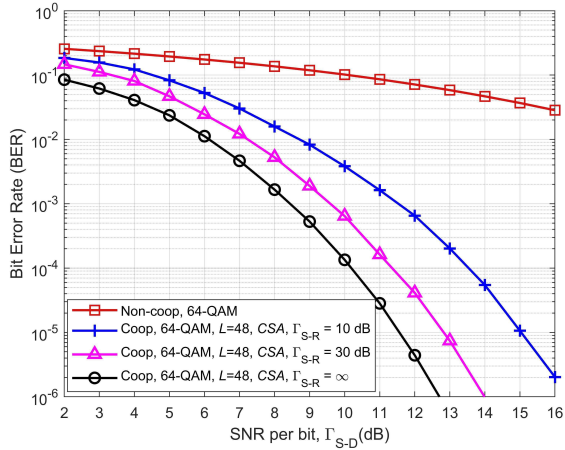


**Fig. 14.** The BER performance of the DRSCC-LD scheme under ideal and non-ideal S-R links compared to the performance of non-cooperative RS coded scheme for the second scenario.

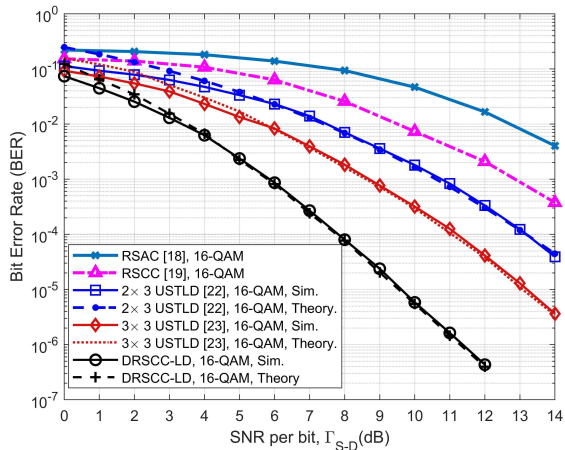


**Fig. 15.** The BER performance of the DRSCC-LD scheme with the existing schemes in [18], [19], [23] and [24]

### 7.5 BER Performance Comparisons of DRSCC-LD Schemes with Other Existing Schemes and the Corresponding Theoretical Analysis Curves

The BER performance comparisons of the DRSCC-LD scheme for the first scenario with the existing schemes, i.e., the RS adaptive cooperation (RSAC) [18], the RS coded cooperative (RSCC) scheme in [19], the  $2 \times 3$  uncoded space-time labeling diversity (USTLD) MIMO scheme in [23] and the  $3 \times 3$  USTLD MIMO scheme in [24] over fast fading channel are plotted in Fig. 15 where the theoretical bounds of the DRSCC-LD scheme based on the (14) and the USTLD schemes in [23] and [24] are included to evaluate the validity of the schemes. As demonstrated in Fig. 15, the proposed DRSCC-LD scheme based on the RC-VSS detection algorithm and the CSA joint decoding algorithm is

superior to the existing schemes. For example, the DRSCC-LD scheme outperforms the RSCC scheme [19] without the LD technique by a gain of approximately 6.8 dB at  $BER \approx 4.1 \times 10^{-4}$  and obtains around 3.5 dB at  $BER \approx 3.7 \times 10^{-6}$  compared with the  $3 \times 3$  USTLD MIMO scheme. Furthermore, at high SNR, the simulation results and ABEP expressions match very closely, demonstrating the dependability of the proposed DRSCC-LD and USTLD schemes in [23], [24].

## 8. Conclusion

In this manuscript, the novel DRSCC-LD scheme over the Rayleigh frequency-flat fast fading channel is proposed to accommodate the wireless communication scenarios. For the proposed scheme, two RS codes with different numbers of consecutive roots and three distinct labeling mappers of 16-QAM and 64-QAM modulation schemes are employed at the source and relay, respectively. To reduce the complexity of the ML detection, the RC-VSS algorithm is present, which provides a good compromise between BER performance and the computational complexity of detection. Based on the RC-VSS algorithm, the signals received at the destination are then further jointly detected. Meanwhile, we also propose a novel joint CSA decoding algorithm at the destination to further improve the overall BER performance. Moreover, the theoretical union bound that closely matches the Monte Carlo simulation result is derived to validate the proposed DRSCC-LD scheme. In the subsequent study, the design of the three different labeling mappers for M-PSK and M-APSK modulation schemes will be explored. Furthermore, the design of selection approach of information sequence at the relay could also be an interesting exploration.

## Acknowledgments

This work was supported by National Natural Science Foundation of China under the contract No. 61771241.

## References

- [1] GOVINDASAMY, K., XU, H. J., PILLAY, N. Space-time block coded spatial modulation with labeling diversity. *International Journal of Communication Systems*, 2017, vol. 31, no. 1, p. 1–15. DOI: 10.1002/dac.3395
- [2] LI, X. D., CHINDAPOL, A., RITCEY, J. A. Bit-interleaved coded modulation with iterative decoding and 8PSK signaling. *IEEE Transactions on Communications*, 2002, vol. 50, no. 8, p. 1250–1257. DOI: 10.1109/TCOMM.2002.801524
- [3] CHINDAPOL, A., RITCEY, J. A. Design, analysis, and performance evaluation for BICM-ID with square QAM constellations in Rayleigh fading channels. *IEEE Journal on Selected Areas in Communications*, 2001, vol. 19, no. 5, p. 944–957. DOI: 10.1109/49.924878
- [4] HUANG, Y. H., RITCEY, J. A. Optimal constellation labeling for iteratively decoded bit-interleaved space-time coded modulation. *IEEE Transactions on Information Theory*, 2005, vol. 51, no. 5, p. 1865–1871. DOI: 10.1109/TIT.2005.846409
- [5] HUANG, Y. H., RITCEY, J. A. Improved 16-QAM constellation labeling for BI-STCM-ID with the Alamouti scheme. *IEEE Communications Letters*, 2005, vol. 9, no. 2, p. 157–159. DOI: 10.1109/LCOMM.2005.02002
- [6] KRASICKI, M. Labelling diversity for MIMO systems. In *European Wireless Conference—Sustainable Wireless Technologies (European Wireless)*. Vienna (Austria), 2011, p. 1–7. ISBN: 9783800733439
- [7] KRASICKI, M. Essence of 16-QAM labelling diversity. *Electronics Letters*, 2013, vol. 49, no. 8, p. 567–569. DOI: 10.1049/el.2012.4275
- [8] VAN DER MEULEN, E. C. Three-terminal communication channels. *Advances in Applied Probability*, 1971, vol. 3, no. 1, p. 120–154. DOI: 10.2307/1426331
- [9] HUNTER, T. E., SANAYEI, S., NOSRATINIA, A. Outage analysis of coded cooperation. *IEEE Transactions on Information Theory*, 2006, vol. 52, no. 2, p. 375–391. DOI: 10.1109/TIT.2005.862084
- [10] ZHAO, C. L., YANG, F. F., UMAR, R., et al. Two-source asymmetric turbo-coded cooperative spatial modulation scheme with code matched interleaver. *Electronics*, 2020, vol. 9, no. 1, p. 1–20. DOI: 10.3390/electronics9010169
- [11] MUGHAL, S., YANG, F. F., UMAR, R. Reed-Muller network coded-cooperation with joint decoding. *IEEE Communications Letters*, 2019, vol. 23, no. 1, p. 24–27. DOI: 10.1109/LCOMM.2018.2879101
- [12] WANG, H., CHEN, Q. C. LDPC based network coded cooperation design for multi-way relay networks. *IEEE Access*, 2019, vol. 7, p. 62300–62311. DOI: 10.1109/ACCESS.2019.2915293
- [13] RIJAL, H., YANG, F. F., RODOR, G. Optimized QC-LDPC coded cooperation for single relay wireless cooperative communication system. In *18th International Computer Conference on Wavelet Active Media Technology and Information Processing (ICCWAMTIP)*. Chengdu (China), 2021, p. 340–343. DOI: 10.1109/ICCWAMTIP53232.2021.9674081
- [14] DIA, D., M., DIOUF, M. D., DIOP, I. Performance of polar codes in cooperative transmission systems. In *Proceedings of 2nd International Conference on Electrical, Communication, and Computer Engineering (ICECCE)*. Istanbul (Turkey), 2020, p. 1–5. DOI: 10.1109/ICECCE49384.2020.9179453
- [15] LIANG, H., LIU, A. J., LIU, X., et al. Construction and optimization for adaptive polar coded cooperation. *IEEE Wireless Communications Letters*, 2020, vol. 9, no. 8, p. 1187–1190. DOI: 10.1109/LWC.2020.2984738
- [16] EJAZ, S., YANG, F. F., XU, H. J. Labeling diversity for 2 x 2 WLAN coded-cooperative networks. *Radioengineering*, 2015, vol. 24, no. 2, p. 470–480. DOI: 10.13164/re.2015.0470
- [17] EJAZ, S., YANG, F. F., XU, H. J. Split labeling diversity for wireless half-duplex relay assisted cooperative communication systems. *Telecommunication Systems*, 2020, vol. 75, no. 4, p. 437–446. DOI: 10.1007/s11235-020-00694-6
- [18] ALMAWGANI, A. H. M., SALLEH, M. F. M. RS coded cooperation with adaptive cooperation level scheme over multipath Rayleigh fading channel. In *IEEE 9th Malaysia International Conference on Communications (MICC)*. Kuala Lumpur (Malaysia), 2009, p. 480–484. DOI: 10.1109/MICC.2009.5431555
- [19] GUO, P. C., YANG, F. F., ZHAO, C. L., et al. Jointly optimized design of distributed Reed-Solomon codes by proper selection in relay. *Telecommunication Systems*, 2021, vol. 78, no. 3, p. 391–403. DOI: 10.1007/s11235-021-00822-w
- [20] ZHAO, C. L., YANG, F. F., CHEN, C., et al. Reed-Solomon coded cooperative space-time block coded spatial modulation. In *International Conference on Wireless Communications and Smart Grid (ICWCSG)*. Hangzhou (China), 2021, p. 99–103. DOI: 10.1109/ICWCSG53609.2021.00027
- [21] AYANDA, D. Performance analysis of M-ary amplitude and phase shift keying uncoded space-time labeling diversity with three transmit antennas in nonlinear Rician. *Transactions on Emerging Telecommunications Technologies*, 2021, vol. 32, no. 11. DOI: 10.1002/ett.4348
- [22] SOLWA, S., ELMEZUGHI, M. K., BAMISAYE, A. J., et al. Genetic algorithm-based uncoded M-ary phase shift keying space-time labelling diversity with three transmit antennas for future wireless networks. In *9th International Conference on Electrical and Electronics Engineering (ICEEE)*. Alanya (Turkey), 2022, p. 423–428. DOI: 10.1109/ICEEE55327.2022.9772544
- [23] XU, H. J., GOVINDASAMY, K., PILLAY, N. Uncoded space-time labeling diversity. *IEEE Communications Letters*, 2016, vol. 20, no. 8, p. 1511–1514. DOI: 10.1109/LCOMM.2016.2580503
- [24] AYANDA, D., XU, H. J., PILLAY, N. Uncoded M-ary quadrature amplitude modulation space-time labeling diversity with three transmit antennas. *International Journal of Communication Systems*, 2018, vol. 31, no. 8, p. 1–13. DOI: 10.1002/dac.3818
- [25] BAHNG, S., SHIN, S., PARK, Y. O. ML Approaching MIMO detection based on orthogonal projection. *IEEE Communications Letters*, 2007, vol. 11, no. 6, p. 474–476. DOI: 10.1109/LCOMM.2007.070146
- [26] BARRY, J. R., LEE, E. A., MESSERSCHMITT, D. G. *Digital Communication*. 3rd ed. Springer US, 2004. ISBN: 9781461502272

## About the Authors ...

**Chen CHEN** (corresponding author) was born in China. She received her B.S degree in Electronic and Information Engineering from Yangzhou University, China, in 2020. She is currently doing the Ph.D. at the College of Electronics and Information Engineering, Nanjing University of Aeronautics and Astronautics, China. Her research interests are circuits and systems, signal processing, and channel coding.

**Fengfan YANG** was born in China. He received his M.Sc. and Ph.D. degrees from the Northwestern Polytechnical University and South-east University, China in 1993, and 1997,

respectively, all in Electronic Engineering. He has been with the College of Information Science and Technology, Nanjing University of Aeronautics and Astronautics since May 1997. From October 1999 to May 2003, he was a research associate at the Centre for Communication Systems Research, University of Surrey, UK, and Dept. of Electrical and Computer Engineering, McGill University, Canada. His major research interests are information theory, channel coding, and their applications for mobile and satellite communications.

**Chunli ZHAO** was born in China. She received her B.S. degree in Electronic and Information Engineering from Henan Normal University Xinlian College, China, in 2014. She obtained her M.Sc. degree in Circuits and Systems at Henan Normal University, China, in 2017. She is currently doing the Ph.D. at the College of Electronics and Information Engineering, Nanjing University of Aeronau-

tics and Astronautics, China. Her research interests are circuits and systems, signal processing, and channel coding.

**Hongjun XU** (MIEEE, 07) was born in China. He received the B.Sc. degree from the University of Guilin Technology, Guilin, China, in 1984; the M.Sc. degree from the Institute of Telecontrol and Telemeasure, Shi Jian Zhuang, China, in 1989; and the Ph.D. degree from the Beijing University of Aeronautics and Astronautics, Beijing, China, in 1995. From 1997 to 2000, he was a Postdoctoral Fellow with the University of Natal, Durban, South Africa, and Inha University, Incheon, Korea. He is currently a full Professor with the School of Engineering at the University of KwaZulu-Natal, Durban. He is also a rated scientist of the national research foundation in South Africa. He has authored and co-authored more than 50 journal papers. His research interests include wireless communications and image processing.